Low-spin collective behavior in the transitional nuclei ^{86,88}Mo

K. Andgren,[1,*] E. Ganioğlu,[1,2] B. Cederwall,[1] R. Wyss,[1] S. Bhattacharyya,[3,†] J. R. Brown,[4] G. de Angelis,[5] G. de France,[3] Zs. Dombrádi,[6] J. Gál,[6] B. Hadinia,[1] A. Johnson,[1] F. Johnston-Theasby,[4] A. Jungclaus,[7] A. Khaplanov,[1] J. Kownacki,[8] K. Lagergren,[9] G. La Rana,[10] J. Molnár,[6] R. Moro,[10] B. S. Nara Singh,[4] J. Nyberg,[11] M. Sandzelius,[1] J.-N. Scheurer,[12] G. Sletten,[13] D. Sohler,[6] J. Timár,[6] M. Trotta,[10] J. J. Valiente-Dobón,[5] E. Vardaci,[10] R. Wadsworth,[4] and S. Williams[14]

[1]*Department of Physics, Royal Institute of Technology, SE-10691 Stockholm, Sweden*
[2]*Science Faculty, Physics Department, Istanbul University, TR-34459 Istanbul, Turkey*
[3]*Grand Accélérateur National d'Ions Lourds (GANIL), CEA/DSM - CNRS/IN2P3, Bd Henri Becquerel, BP 55027, F-14076 Caen Cedex 5, France*
[4]*Department of Physics, University of York, YO10 5DD York, United Kingdom*
[5]*I.N.F.N., Laboratori Nazionali di Legnaro, I-35020 Legnaro, Italy*
[6]*ATOMKI, H-4001 Debrecen, Hungary*
[7]*Departamento de Física Teórica, Universidad Aut'onoma de Madrid, E-28049 Madrid, Spain*
[8]*Heavy Ion Laboratory, Warsaw University, PL-02-093 Warsaw, Poland*
[9]*Joint Institute for Heavy-Ion Research, Holifield Radioactive Ion Beam Facility, Oak Ridge, Tennessee 37831, USA*
[10]*Dipartimento di Scienze Fisiche, Università di Napoli and INFN, I-80126 Napoli, Italy*
[11]*Department of Nuclear and Particle Physics, Uppsala University, SE-75121 Uppsala, Sweden*
[12]*Université Bordeaux 1, CNRS/IN2P3, Centre d'Etudes Nucláires de Bordeaux Gradignan, UMR 5797, Chemin du Solarium, BP120, F-33175 Gradignan, France*
[13]*The Niels Bohr Institute, University of Copenhagen, 2100 Copenhagen, Denmark*
[14]*TRIUMF, Vancouver, British Columbia, V6T 2A3, Canada*

(Received 15 March 2007; published 16 July 2007)

Low-spin structures in ^{86,88}Mo were populated using the ^{58}Ni(^{36}Ar, $x\alpha yp$) heavy-ion fusion-evaporation reaction at a beam energy of 111 MeV. Charged particles and γ rays were emitted in the reactions and detected by the DIAMANT CsI ball and the EXOGAM Ge array, respectively. In addition to the previously reported low-to-medium spin states in these nuclei, new low-spin structures were observed. Angular correlation and linear polarization measurements were performed in order to unambiguously determine the spins and parities of intensely populated states in ^{88}Mo. Quasiparticle Random Phase Approximation (QRPA) calculations were performed for the first and second excited 2^+ states in ^{86}Mo and ^{88}Mo. The results are in qualitative agreement with the experimental results, supporting a collective interpretation of the low-spin states for these transitional nuclei.

DOI: 10.1103/PhysRevC.76.014307 PACS number(s): 23.20.Lv, 23.20.En, 27.50.+e, 29.30.Kv

I. INTRODUCTION

Neutron deficient nuclei with proton numbers $Z > 40$ and neutron numbers near the closed neutron shell at $N = 50$ have been the targets of extensive research in the past; see for instance [1]. These isotopes lie in the transitional region between the well deformed nuclei at $Z \approx 38, N \approx 38$, exhibiting collective excitation modes, and the nuclei with $N > 46$, which are well described by the spherical nuclear shell model. The degree of collectivity changes dramatically with changing nucleon numbers in this mass region of the nuclear chart. For example, the low-lying yrast states of even-even neutron deficient molybdenum isotopes with $N < 46$ have been described within the collective rotational model, as in the case of ^{86}Mo [2], whereas the more neutron-rich isotopes ^{90,92}Mo in the vicinity of the $N = 50$ shell closure can be described by spherical shell-model calculations [3]. A systematic study by Gross *et al.* [4] of the neutron-deficient molybdenum isotopes indicates that ^{88}Mo is best described as a transitional nucleus with a combination of collective and single-particle excitations. Weiszflog *et al.* [5] confirmed the interpretation of the low-lying states in this nucleus as being built on a spherical ground state with the excited states well explained within the spherical shell model. Another systematic study of the $N = 46$ isotones by Galindo *et al.* [6] also supports the shell-model description of ^{88}Mo. However, reduced transition probabilities derived from measured lifetimes of the yrast low-spin states in this nucleus [7] indicate a collective nature for the 4^+ and the 2^+ levels. These findings suggest that the low-lying structures of ^{88}Mo are highly complex and it is therefore of interest to search for other low-spin states in this nucleus, which may give additional information on its excitation modes and shed light on the transitional behavior of this nucleus.

II. EXPERIMENT

Low-spin states in ^{86,88}Mo were studied via ^{58}Ni(^{36}Ar, $x\alpha yp$)^{86,88}Mo fusion-evaporation reactions. The ^{36}Ar beam was delivered by the GANIL CIME cyclotron at a beam energy of 111 MeV and with an intensity of 5 particle nA. The

*Corresponding author: andgren@nuclear.kth.se
†Present address: V.E.C.C, 1/AF Bidhan Nagar, Kolkata 700064, India.

target consisted of a 99.9% isotopically enriched ^{58}Ni foil. The target thickness was 6.0 mg/cm^2, which was enough to stop the fusion products. Charged-particle emission following the decay of the ^{94}Pd compound nucleus was detected using the DIAMANT [8,9] detector system which consisted of 80 CsI scintillators. The Neutron Wall, comprising 45 liquid scintillator detectors [10] and covering a solid angle of 1π in the forward direction, was used for the detection of evaporated neutrons. Gamma rays emitted from the reaction products were detected using the EXOGAM [11–13] Ge detector system. At the time of the experiment, six segmented clover detectors were placed at an angle of 90° and four detectors at an angle of 135° relative to the beam direction, leaving room for the Neutron Wall at forward angles. EXOGAM was used in a close-packed configuration with the front part of the BGO Compton suppression shields removed from the clover detectors. The trigger condition was fulfilled if either two or more γ rays were detected in coincidence in the Ge detectors or if one or more γ rays were registered together with at least one neutron in the Neutron Wall.

In the off-line analysis, the selected events contained two detected alpha particles (corresponding to the production of ^{86}Mo) or one detected alpha particle together with two detected protons (corresponding to ^{88}Mo). The α particle and proton detection efficiencies were estimated to 48(2)% and 55(2)%, respectively. The efficiency for detecting protons was smaller than usual in this experiment, since the backward DIAMANT detectors could not be used for particle selection due to noise induced by back-scattered ions. This did not significantly affect the detection efficiency for α particles, since these are mainly emitted in the forward directions due to the kinematical focusing. The particle condition of 2α was fulfilled by 1.3×10^6 events, and the condition of $1\alpha2p$ by 2.1×10^7 events. In the events selected with the condition of two detected α particles, approximately 85% belonged to ^{44}Ti produced via reactions of ^{36}Ar on ^{16}O. The oxygen contamination is present, since the "vacuum" in the beam line and the target chamber is not ideal. In the events where one α particle was detected together with two protons, approximately 20% belonged to ^{46}Ti produced via reactions on ^{16}O. Based on the experimental information, the cross section for the reactions producing ^{88}Mo was estimated to be of the order of one mb and the cross section for producing ^{86}Mo was 8% relative to that of ^{88}Mo.

III. DATA ANALYSIS

The events satisfying the trigger condition were written to magnetic tape and analyzed off-line. For the detected charged particles the CsI detectors give three parameters: the energy, the time, and the "particle identification". The "particle identification" (pid) spectra are obtained from the pulse shape using the rise time combined with the zero-crossover method [14]. Prompt protons and alpha particles were chosen by simultaneous selection criteria for the pid and the time parameters. Conditions for the energy and the pid parameters were also applied in order to differentiate between protons and alpha particles. Gamma rays were required to be escape-suppressed and detected in prompt coincidence

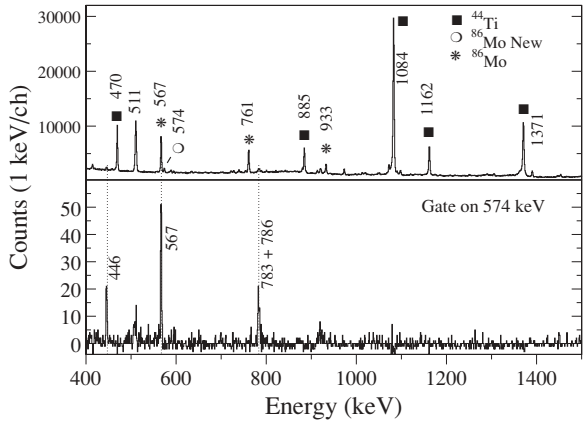

FIG. 1. The upper spectrum shows the total projection of the E_γ-E_γ matrix, sorted with the condition of two detected alpha particles together and zero detected protons. The lower panel shows a background subtracted spectrum of γ rays detected in coincidence with the 574 keV γ ray, corresponding to the transition that depopulates the 2_2^+ state in ^{86}Mo.

with the RF-pulse from the cyclotron. To further reduce the background originating from Compton scattered photons, the energies extracted from individual coincident pulses from the four crystals belonging to one clover were added. The resulting γ-ray energies recorded by the Ge clover detectors were then sorted into E_γ-E_γ coincidence matrices for ^{86}Mo and ^{88}Mo, with the appropriate particle conditions, and an E_γ-E_γ-E_γ cube was constructed for ^{88}Mo. The matrices and the cube were analyzed using the software programs ESCL8R and LEVIT8R [15,16]. Figure 1 shows the total projection of the 2α-selected matrix, as well as the projection spectrum when γ rays coincident with the 574 keV transition in ^{86}Mo are selected (see Sec. IV A for the level scheme). Figure 2 shows the corresponding total projection of the matrix with the charged particle condition of $1\alpha2p$ together with the projection

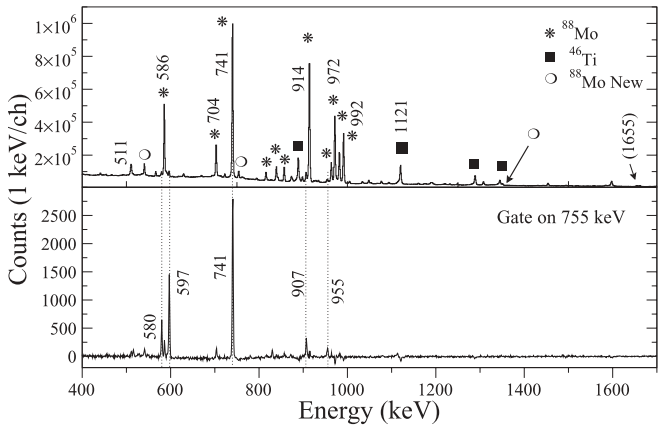

FIG. 2. The upper spectrum shows the total projection of the E_γ-E_γ matrix sorted with the condition of two detected protons and one detected alpha particle. The lower panel shows a background subtracted spectrum of γ rays detected in coincidence with the 755 keV γ ray, corresponding to the transition that depopulates the 2_2^+ state in ^{88}Mo.

TABLE I. Spin assignments, level energies, γ-ray energies, and intensities relative to the $2_1^+ \rightarrow 0^+$ 567 keV transition, of transitions observed for the first time in ^{86}Mo.

I_i^π ($\hbar$)	I_f^π ($\hbar$)	E_x (keV)	E_γ (keV)	$I_{\rm rel}$ %
(2_2^+)	2_1^+	1141.6(1)	574.3(1)	11(1)
(3^+)	(2_2^+)	1587.8(3)	446.2(2)	7(1)
(4_2^+)	(2_2^+)	1924.1(4)	782.5(3)[a]	≈5
(5^+)	(3^+)	2373.5(4)	785.7(3)[a]	≈5

[a]Doublet character.

spectrum when γ rays coincident with the 755 keV transition in ^{88}Mo are selected (see Sec. IV B for the level scheme).

The relative intensities (as noted in the Tables I, II, and III) of the γ rays were obtained from the total projection spectra of the matrices. If the peak-to-background ratio in the total projection spectra was too low, or if there was contamination in the peak from other γ-ray transitions, the relevant transition energies were selected in the coincidence matrices and the obtained projection spectra was used to fit the relative intensities. The energies of the transitions were also measured in the total projection spectra in the matrices. The energy uncertainties presented in the tables are a sum of statistical, calibration and background errors.

Coincident γ rays may accidentally be summed up when using the clover detectors in add-back mode. In order to check for the contribution of such events in the spectra, the intensity of the 1655 keV peak (indicated in Fig. 2) in the projection sorted with the selection criterion of $1\alpha 2p$ corresponding to ^{88}Mo was analyzed and compared to the intensities of the 741 ($2_1^+ \rightarrow 0^+$) and the 914 keV ($4^+ \rightarrow 2_1^+$) transitions of ^{88}Mo. The 1655 keV peak was not seen in coincidence with the 741 or the 914 keV transition, however, the peak was in coincidence with the 972 and the 992 keV transitions confirming that it is indeed most probably caused by summing. An upper limit for the contribution from energy summing to the reported intensities could thus be estimated to 0.9%.

In order to assign spins to the energy levels, the ratios of directional correlation of oriented states (DCO ratios) [17] for the transitions were deduced according to

$$R_{\rm DCO} = \frac{I(\gamma_1 \text{at} 135^\circ;\ \text{gated by}\ \gamma_2\ \text{at}\ 90^\circ)}{I(\gamma_1\ \text{at}\ 90^\circ;\ \text{gated by}\ \gamma_2\ \text{at}\ 135^\circ)}. \quad (1)$$

The data were sorted into a particle-gated matrix with the γ rays detected in the four clover detectors at 135° on one axis and the γ rays detected in the six clover detectors at 90° on the other axis. The detection efficiency as a function of photon energy had similar shape for the two detector angles for transition energies above 250 keV. Since all transition energies of interest for this analysis were larger than 250 keV, no efficiency correction of the measured intensities was needed in order to obtain the correct DCO ratios.

A. Polarization measurements

Angular distribution (or correlation) measurements of the emitted γ rays are often used when assigning spins and parities to excited levels. Such measurements can distinguish between transitions of different multipole orders, but do not provide information on whether a transition is of electric or magnetic type. This information can, if the experimental setup allows, be obtained through linear polarization measurements as described in Ref. [18]. The Ge clover detectors of the EXOGAM array are suitable as Compton polarimeters. For example, the 2647 keV level in ^{88}Mo has previously been assigned a spin-parity of $I^\pi = 5^-$ [5,7], which agrees well with predictions from the spherical shell model. However, the experimental assignment is based only on DCO ratios and angular distribution measurements, which indicate a stretched dipole character for the depopulating 992 keV transition. This would be consistent with a spin assignment of 5^+ in addition to 5^- for this state. We have determined the spin and parity

TABLE II. Spin assignments, level energies, γ-ray energies, intensities relative to the $2_1^+ \rightarrow 0^+$ 741 keV transition, DCO ratios, and scattering asymmetries [as defined by Eq. (2)] of previously reported transitions in ^{88}Mo. The gates used for determination of the DCO ratios and the asymmetries are indicated in the table.

I_i^π ($\hbar$)	I_f^π ($\hbar$)	E_x (keV)	E_γ (keV)	$I_{\rm rel}$ %	$R_{\rm DCO}$	Gate$_{\rm DCO}$ (keV)	Asymmetry	Gate$_{\rm Asymmetry}$[a]
2_1^+	0^+	740.6(1)	740.6(1)	100	1.12(3)	840+899[b]	+0.07(1)	A
4^+	2_1^+	1655.1(1)	914.5(1)	90.5(11)	1.00(1)	741	+0.08(1)	A
6^+	4^+	2627.1(2)	972.1(1)	48.1(8)	1.00(1)	741	+0.09(1)	A
8_1^+	6^+	3213.4(2)	586.3(1)	39.8(7)	1.04(1)	741	+0.10(2)	A
8_2^+	8_1^+	3484.9(2)	271.5(1)	6.3(10)	1.09(4)	741	+0.2(1)	A
10_1^+	8_1^+	4195.8(2)	982.4(1)	24.2(5)	0.92(2)	741	+0.07(2)	A
10_2^+	8_2^+	4358.6(3)	873.7(3)	3.6(8)	1.09(5)	741+586	+0.15(7)	A
12_1^+	10_1^+	5053.2(2)	857.5(1)	13.0(5)	0.98(3)	741	+0.09(4)	A
5^-	4^+	2646.8(1)	991.7(1)	35.9(7)	0.68(1)	741	+0.05(1)	A
7^-	5^-	3350.3(1)	703.5(1)	21(1)	0.98(2)	741	+0.08(2)	A
9^-	7^-	4314.4(2)	964.2(1)	14.2(4)	1.14(3)	741	+0.06(2)	A
11^-	9^-	5154.1(4)	839.7(3)	12.0(4)	1.00(4)	741	+0.13(3)	A

[a]A: 741 + 914 keV.
[b]$15^- \rightarrow 13^-$ transition from the 6868 keV state.

TABLE III. Spin assignments, level energies, γ-ray energies, intensities relative to the $2_1^+ \rightarrow 0^+$ 741 keV transition, DCO ratios, and scattering asymmetries [as defined by Eq. (2)] of not previously reported transitions in ^{88}Mo. The gates used for determination of the DCO ratios and the asymmetries are indicated in the table.

I_i^π ($\hbar$)	I_f^π ($\hbar$)	E_x (keV)	E_γ (keV)	I_{rel} %	R_{DCO}	Gate_{DCO} (keV)	Asymmetry	$\text{Gate}_{\text{Asymmetry}}$[a]
2_2^+	2_1^+	1495.1(1)	754.5(1)	4.4(3)	1.0(1)	741		
2_2^+	0^+	1495.1(1)	1495.0(6)	0.6(2)				
3^+	2_2^+	2092.0(2)	596.9(2)	2.6(3)	1.3(2)	741	−0.06(5)	A
3^+	2_1^+	2092.0(2)	1351.2(4)	1.6(3)	0.9(1)	741		
	2_2^+	2402.2(2)	907.1(1)2[b]	0.8(1)				
(5^+)	3^+	2672.1(3)	580.1(2)	2.3(3)	1.0(1)	741		
	3^+	3047.0(3)	955.0(2)2[b]	0.9(1)				
(6_1^-)	5^-	3188.0(2)	541.2(1)	6.2(4)	0.5(1)	914	<0.05	B
(6_2^-)	5^-	3213.7(2)	567.0(2)	2.0(3)	0.7(1)	914	<0.06	B
	(6_1^-)	3642.8(3)	454.8(3)	0.5(1)				
(8^-)	(6_2^-)	4064.0(5)	850.2(4)	0.5(1)				
(8^-)	(6_1^-)	4064.0(4)	876.1(2)	1.1(2)				
(10^-)	(8^-)	4989.1(5)	925.0(3)	0.9(1)				
9^-	7^-	3663.3(2)	313.1(1)	2.6(5)	1.07(10)	741	+0.2(1)	C
	(9^-)	5270.6(4)	956.2(3)2[b]	0.6(1)				

[a]A: 741 + 755 + 597 + 580 keV, B: 741 + 914 + 992 + 877 + 850 + 455 + 925 keV, C: 741 + 914 + 704 keV.
[b]Doublet character.

of this state to 5^- by measuring the linear polarization of the 992 keV transition.

The asymmetry of Compton-scattered polarised photons is given by

$$A = \frac{I_v - I_h}{I_v + I_h}, \tag{2}$$

where I_v is the intensity of vertically Compton-scattered photons and I_h is the intensity of horizontally Compton-scattered photons. The reference plane determining the scattering direction is spanned by the beam direction and the direction of the emitted γ ray. The polarization, P, is given by the ratio between the asymmetry and the polarization sensitivity, Q. The value of Q depends on the geometry of the experimental setup and it also decreases with increasing energy of the γ ray. The absolute value of the asymmetry is typically $\lesssim 0.1$. Because this technique requires relatively high statistics, no conclusive polarization measurements were possible for ^{86}Mo. The clover detectors situated at 90° relative to the beam axis were used when measuring I_v and I_h, since they are the most sensitive to the asymmetry [18]. The γ rays were sorted into two matrices with photons producing a signal in only one of the four crystals belonging to the same clover on the x-axis and vertically or horizontally scattered photons (producing signals in two out of the four clover crystals) on the y-axis. The γ ray energies on the x-axis had been detected in the clover detectors both at 90° and 135° in order to increase the statistics. The asymmetry, defined in Eq. (2), is negative for stretched, purely magnetic transitions, while it is positive for stretched, purely electric transitions. The inset in Fig. 3 illustrates this method applied to the strongest reaction channel in the present experiment, the $3p$ channel leading to ^{91}Tc [19], which has previously established transitions of both electric and magnetic type.

IV. RESULTS

A. ^{86}Mo

New γ rays assigned to ^{86}Mo are listed in Table I. Poor statistics precluded angular correlation and polarization measurements for the γ rays of this reaction channel. Spin-parity assignments for the new levels are based on the systematics in the neighboring isotopes. A partial level scheme of ^{86}Mo as obtained from this work, together with the systematics of low-lying states in ^{88,90}Mo, is shown in Fig. 4.

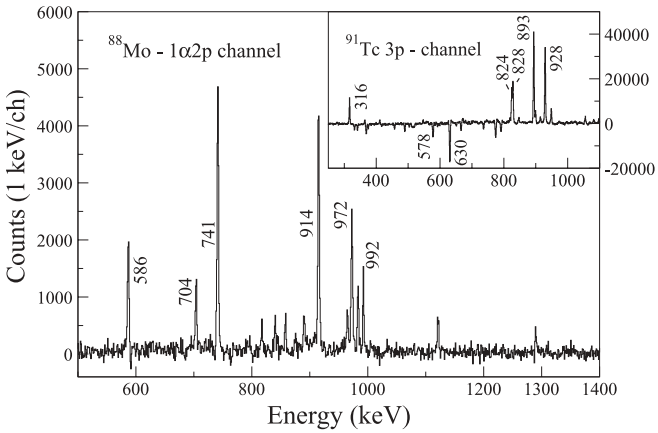

FIG. 3. The projection containing the vertically scattered γ rays subtracted by the projection containing the horizontally scattered γ rays. These γ rays were detected in coincidence with one α particle and two protons. The spectrum for ^{91}Tc (inset) clearly shows both positive and negative peaks in the subtracted spectra, corresponding to stretched electric and magnetic transitions, respectively.

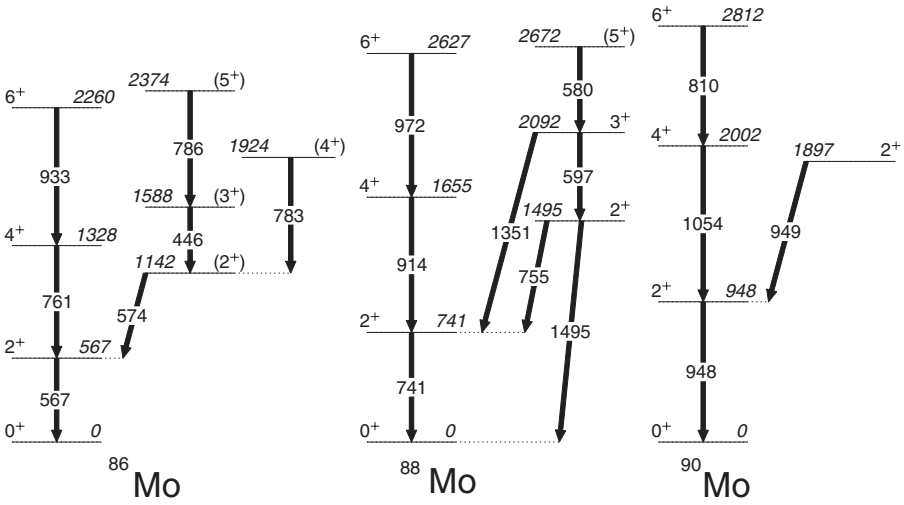

FIG. 4. The first three transitions in the ground state bands and the second excited 2_2^+ states in ^{86,88,90}Mo. The states in ^{90}Mo have been observed previously [20,21]. The side structures in ^{86,88}Mo have been observed for the first time in this work.

B. ^{88}Mo

New γ rays assigned to ^{88}Mo are listed in Table III, and the known γ rays whose asymmetry have been measured in this work are listed in Table II. The partial level scheme, which is shown in Fig. 5, was obtained by combining the results from the analysis of the E_γ-E_γ coincidence matrix and the E_γ-E_γ-E_γ cube. The spin assignments, when permitted by statistics, are based on measured Compton asymmetries and DCO ratios for the transitions.

All previously reported γ ray transitions have positive asymmetry, which means they have a stretched electric character or a nonstretched magnetic character. Most DCO ratios are close to unity, implying that the transitions have a stretched $E2$ character or a nonstretched $M1$ character. The exception is the 992 keV transition, for which the DCO ratio points toward a stretched dipole character. Together with the results from the polarization measurements, this leads to the unambiguous assignment of 5^- for the 2647 keV level. The DCO ratio of the 992 keV transition of 0.68(1) is hence the expected ratio for a pure stretched dipole transition, since $I_i \rightarrow I_i - 1$ parity-changing transitions have a very small contribution from higher multipole orders.

In the case of the new 2_2^+ state at an excitation energy of 1495 keV, a gate was set in the DCO matrix on the stretched 741 keV $E2$ transition to the ground state. The DCO ratio of 1.0(1) for the 755 keV transition following the decay of the 2_2^+ state is consistent with both a nonstretched dipole transition and a stretched quadrupole transition. The 1495 keV transition to the ground state, however, confirms the spin-parity assignment: if the state had a negative parity ($I^\pi = 2^-$), or if the spin-parity of the state were 4^+, the 1495 keV transition would be expected to be significantly weaker. For the state at 2092 keV, which decays via a 597 keV transition to the 2_2^+ state or via a 1351 keV transition to the 2_1^+ state, the measured DCO ratio for the 597 keV transition indicates a mixed $M1/E2$ transition. The scattering asymmetry is also consistent with this and we therefore assign the spin and parity 3^+ to this state. The 580 keV γ ray feeding the 3^+ state has a DCO ratio consistent with a stretched quadrupole character, although the possibility of a mixed $M1/E2$ transition cannot be ruled out. The polarization measurement for this γ ray is inconclusive and the assignment of 5^+ to this level is therefore tentative. The spin assignments of the positive-parity states are consistent with the systematics of the $N = 46$ isotones, as displayed in Fig. 6. The spin and parity of the two remaining observed positive parity states, decaying via 907 and 955 keV transitions to the 2_2^+ and the 3^+ states, could not be determined due to lack of statistics. The gates used for the asymmetries and DCO ratios are indicated in Tables II and III.

The two new transitions (541 and 567 keV) feeding into the 5^- level have DCO ratios that indicate a stretched dipole character. Unfortunately the sign of the asymmetry for these γ rays could not be determined due to insufficient statistics. However, the absolute value of the asymmetry can be used to differentiate between dipole and quadrupole transitions. The measured asymmetry of the 586 keV $8^+ \rightarrow 6^+$ $E2$ transition of 0.10(2) makes it possible to evaluate the expected asymmetry for dipole transitions from $I_i = 6\hbar$ to $I_f = 5\hbar$ at this energy [22,23]. Assuming a spin alignment of $\sigma/J = 0.3$ leads to an asymmetry value of 0.03 for pure stretched dipole transitions. The asymmetry of the 541 and the 567 keV transitions of < 0.06 supports a dipole character for these transitions. We suggest a tentative spin and parity $I^\pi = 6^-$ for the two states decaying with 541 keV and 567 keV, based on the systematics in this region [2,24,25]. The statistics were insufficient for DCO ratios and polarization measurements for the γ-ray transitions between the higher-lying states in this structure, for which spin assignments are tentative.

V. DISCUSSION

A. Positive parity states in ^{86,88}Mo

Several new nonyrast low-energy positive-parity states have been identified in ^{86}Mo and ^{88}Mo. The low-energy levels have been grouped into positive-parity structures. The new structures are interpreted as being built on a γ-vibrational 2^+ state at 1142 and 1495 keV in the two isotopes. For ^{86}Mo, the spin-parity assignment of the second excited 2^+ state is based solely on the systematics of the $N = 44, 46$ isotones. The spin-parity assignment of the states in ^{88}Mo is based on the measured DCO ratios and the polarization measurements

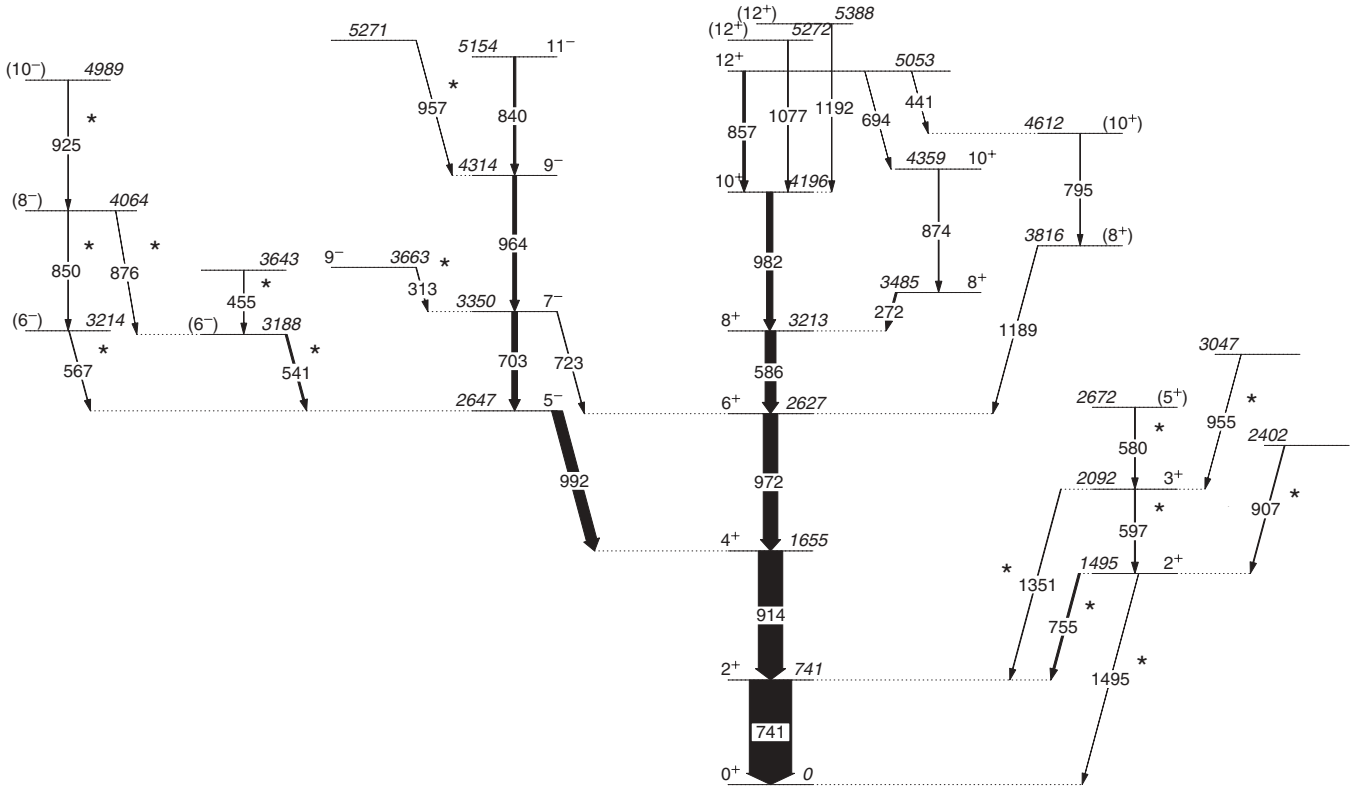

FIG. 5. Partial level scheme of ^{88}Mo as obtained from the present experiment. The new transitions are marked by stars.

from this experiment. The second 2^+ state has not been observed before in any molybdenum isotope with $N \leqslant 46$. However, positive-parity states similar to the sequences in ^{86,88}Mo have been observed in the $N = 44$ isotones ^{80}Kr [26], ^{82}Sr [27], and ^{84}Zr [25], as well as in the $N = 46$ isotones ^{82}Kr [28], ^{84}Sr [29], and ^{86}Zr [24,30]. Although the Mo isotopes show great similarities to each other, the resemblance to the $N = 44, 46$ isotonic chains with different proton numbers is even more striking. For the neutron-deficient $N = 44$ isotones, the excitation mode of the low-spin states is clearly of a collective character with relatively low energies of the 2^+ states, $\approx$ 600 keV (compared with $\approx$ 750 keV for the $N = 46$ isotones), and large $B(E2 : I \rightarrow I - 2)$ values for the same states (39.5(25), 48(2) and 33(3) W.u. for ^{80}Kr [31], ^{82}Sr [27], and ^{84}Zr [32], respectively) compared with the values for the $N = 46$ isotones. However, for the $N = 46$ isotones, with two neutron holes fewer in the $g_{9/2}$ shell, the theoretical interpretation of the low-energy levels is not straightforward. Both shell model calculations and collective models have been used to explain the structures of these isotones. A comparison between the low-lying positive-parity states and their decay patterns in the $N = 46$ nuclei are shown in Fig. 6.

The levels built on the second 2^+ state in ^{88}Mo show a pattern similar to the nuclei with lower proton numbers, suggesting that the proton number does not affect these structures significantly.

Information on the reduced transition probabilities, $B(E2)$ values, is important for determination of the nuclear excitation mode. An increase of the angular momentum due to single-particle excitations typically gives a $B(E2)$ value of a few Weisskopf units (W.u.), whereas a $B(E2)$ value larger than 10 W.u. indicates a collective excitation mode. The change in reduced transition probability as a function of spin can be used to differentiate between vibrational and rotational collective excitations. Rotational nuclei show large and close to constant $B(E2)$ values as a function of spin, whereas vibrational nuclei have increasing $B(E2)$ values as a function of spin. The yrast 2^+ and 4^+ states built on the ground state in ^{82}Kr have been interpreted as rotational excited levels because of their large $B(E2 : I \rightarrow I - 2)$ values [21(1) and 11–42 W.u., respectively [28]. As the angular momentum increases the influence of single-particle excitations becomes more important. The ground-state band up to spin 6^+ and the γ-vibrational band in ^{84}Sr have furthermore been interpreted in terms of collective rotational excitations (with some mixing of two quasiparticle states) due to the large and almost constant $B(E2)$ values for the 2^+, 4^+, and 6^+ states [26(3), 17(2), and 21(3) W.u. [29]. The reduced transition probabilities of the yrast 2^+, 4^+, and 6^+ states in ^{86}Zr have been deduced to 14(3), 7(3), and 3(2) W.u. and the states have been interpreted as single-particle shell-model excitations with some softness to vibration for the 2^+ state [24,33]. The $B(E2)$ values for the low-spin yrast states, 2^+, 4^+, and 6^+ in ^{88}Mo were deduced to 15(1), 40(6), and 3(1) W.u. [7]. The $B(E2)$ value for the 6^+ state is indicating a single-particle excitation for this state, whereas the large increase in the $B(E2)$ value from the 2^+ to the 4^+ state supports a collective quadrupole vibrational description of these states. Also the $E(4^+)/E(2^+)$ ratio of $\approx$ 2.2 supports an interpretation of these levels in terms of near-harmonic vibration.

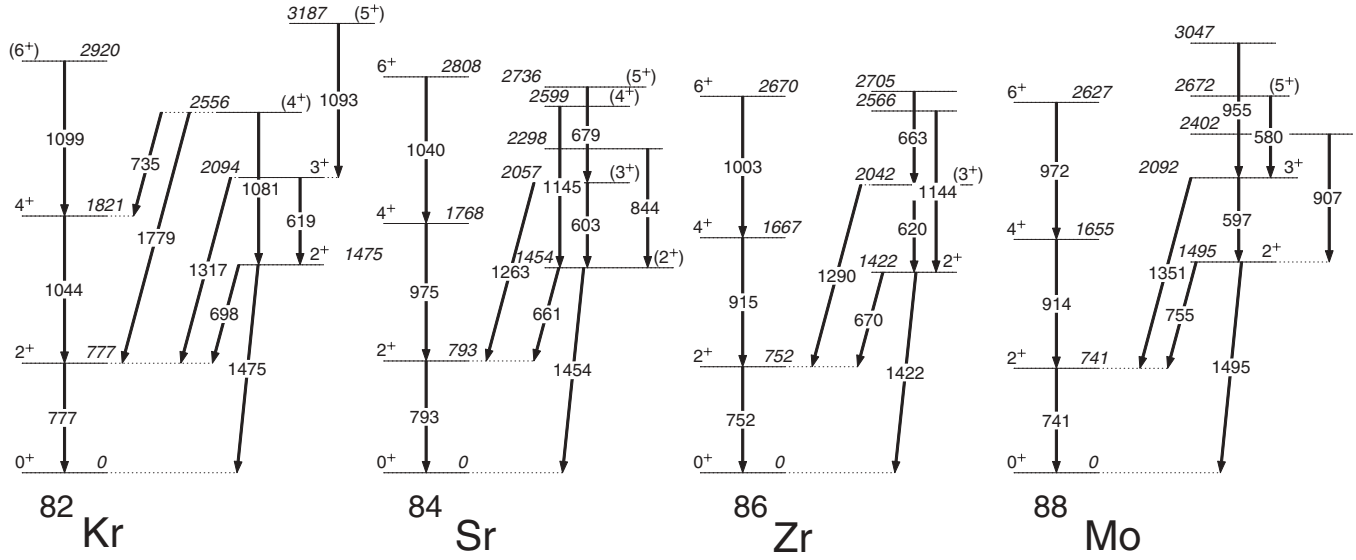

FIG. 6. The ground-state band and the states built on the second excited 2_2^+ state in the $N = 46$ isotones.

B. QRPA calculations

Quasiparticle random phase approximation (QRPA) [34] calculations were performed for the first and the second excited 2^+ states in ^{86,88,90}Mo. QRPA calculations have proved to sensitively describe low-lying vibrational excitations in the harmonic approximation. They are hence very useful to indicate changes from collective excitations to single-particle excitations as well as the onset of static deformation. In this study, we compare the calculated excitation energies to the measured values in Fig. 7. In our calculations [35], the QRPA solutions are based on the deformation values obtained from the mean field solution of the Woods-Saxon single particle potential [36] and the Strutinsky shell correction approach [37]. The calculated pairing gaps from the QRPA solution were adjusted to the experimental pairing gaps as an initial check of the chosen pairing strength parameters. When solving the QRPA equations, many symmetries such as translational invariance, isospin symmetry and rotational invariance are broken by the Hartree-Fock solution. The broken symmetries give rise to a spurious 1^+ state that does not correspond to any physical excitations [38]. The spurious mode was adjusted to zero energy by correction of the residual interaction strength [39]. The model predicts the energy of the first excited vibrational states, normally associated with β- and γ vibrations.

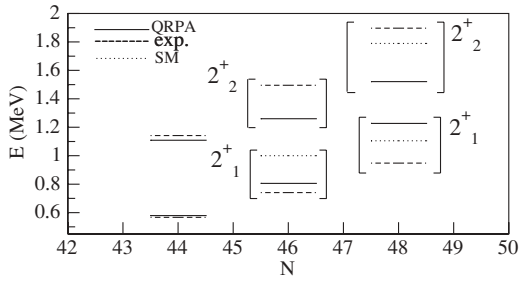

FIG. 7. Calculated level energies, using the QRPA model, of the first and the second excited 2^+ states in ^{86,88,90}Mo. The first 2^+ state corresponds to a β vibration and the second 2^+ state corresponds to a γ vibration in the calculations. Calculated level energies using the spherical shell model are also shown, the values are taken from Refs. [6,7]. The theoretical predictions are compared to experimental data based on this work.

Figure 7 shows that the model qualitatively describes the trend of increasing excitation energies of the first excited 2^+ states in the Mo chain. For ^{86}Mo there is also a good quantitative agreement between the calculated and the measured excitation energies of the 2_1^+ and the 2_2^+ states. However, with increasing neutron number, N, the agreement between the theoretical predictions and the experimental values becomes gradually worse and the calculations fail to reproduce the trend of the second 2^+ state. The previously reported shell model calculations of the 2_1^+ state in ^{88}Mo [6] and the two lowest-lying 2^+ states in ^{90}Mo [7] are also presented in Fig. 7. The results of these calculations show a fairly good agreement for the $N = 48$ nucleus ^{90}Mo, whereas the QRPA model works better for the transitional nucleus ^{88}Mo. Total Routhian surface calculations at a rotational frequency of $\hbar\omega \approx 0.3$ MeV for ^{86,88}Mo have been performed by Gross [4]. The results give soft surfaces for both isotopes, with a triaxial minimum at ($\beta_2 = 0.27, \gamma = -30°$) for ^{86}Mo and a spherical minimum for ^{88}Mo. The low-spin states of the γ-soft deformed nucleus ^{86}Mo are easily explained using collective models, such as the QRPA model. However, as the neutron number is approaching the $N = 50$ shell closure the nuclear shape is predicted to become spherical, and for the transitional nucleus ^{88}Mo it has not been clear whether the low-spin states can best be described as vibrations around a spherical minimum or as single-particle excitations within a shell-model context. The agreement between our QRPA calculations and the experiment for ^{88}Mo indicates that the 2^+ states in this nucleus can be described using a collective quadrupole vibrational model.

C. Negative parity states in ^{88}Mo

Low-lying negative parity states in ^{88}Mo can be constructed as two quasi-particle configurations of the type $(2p_{1/2}1f_{5/2}, 1g_{9/2})$. Indeed, low-lying $I^{\pi} = 5^{-}$ states have been observed in the neutron-deficient isotopes ^{86,88,90}Mo [2,3,5]. The lowest negative-parity state with an even spin is low in energy (the 6^{-} state is only 242 keV above the 5^{-} state) in ^{86}Mo [2]. This might reflect the larger number of valence neutrons compared with ^{90}Mo, with only four valence particles, where the energies of the even-spin negative-parity states are further away from the yrast line and the lowest confirmed even-spin state above the 5^{-} state has a value of $I = 10\hbar$. States with a spin-parity assignment of 6^{-}, have been observed in the $N = 46$ isotones ^{82}Kr, ^{84}Sr, and ^{86}Zr [24,28,29], and the energy of these states are 500–600 keV above the 5^{-} states. The new even-spin states, tentatively assigned as 6^{-} states, observed in ^{88}Mo lie at 541 and 569 keV above the 5^{-} state and are presumed to consist of neutron and proton $(1f_{5/2}, 1g_{9/2})$ two-quasiparticle configurations.

VI. CONCLUSIONS

Excited levels in ^{86}Mo and ^{88}Mo were populated via the reactions ^{58}Ni(^{36}Ar, $x\alpha yp$)^{86,88}Mo at a beam energy of 111 MeV. New low-lying energy levels with positive parity were observed in both nuclei and for ^{88}Mo negative-parity even-spin states were tentatively observed for the first time. Where permitted by statistics, spins and parities were assigned to the new levels and for previously reported levels in ^{88}Mo, by measuring the DCO ratios and the linear polarisations of the γ rays. The new low-spin positive-parity structures in ^{86}Mo and in ^{88}Mo are interpreted as excitation modes built on γ-vibrational 2^{+} states. The presence of these new vibrational states, which are interpreted within the QRPA model, together with the large and increasing $B(E2)$ values of the yrast low-spin states in ^{88}Mo establish the low-energy excitation modes in both nuclei as being of a collective character.

ACKNOWLEDGMENTS

The authors would like to thank Lars Einarsson for providing some of the targets used in this experiment and the operators of the GANIL Cyclotrons for providing the ^{36}Ar beam. We would also like to thank N. Alahari and other members of the E403aS collaboration for setting up and optimising the EXOGAM and the Neutron Wall system at GANIL. Further support for this work has been provided by the Swedish Research Council, the U.K. Engineering and Physical Sciences Research Programme "Interacting Infrastructure Initiative—Transnational Access", Contract No. RII3-CT-2004-506065 (EURONS), project no. OTKA T046901, and the Spanish Ministerio de Educación y Ciencia, Contract No. FPA2005-00696.

[1] D. Rudolph, K. P. Lieb, and H. Grawe, Nucl. Phys. **A597**, 298 (1996).
[2] D. Rudolph, C. J. Gross, Y. A. Akovali, C. Baktash, J. Döring, F. E. Durham, P.-F. Hua, G. D. Johns, M. Korolija, D. R. LaFosse, I. Y. Lee, A. O. Macchiavelli, W. Rathbun, D. G. Sarantites, D. W. Stracener, S. L. Tabor, A. V. Afanasjev, and I. Ragnarsson, Phys. Rev. C **54**, 117 (1996).
[3] P. Singh, R. G. Pillay, J. A. Sheikh, and H. G. Devare, Phys. Rev. C **45**, 2161 (1992).
[4] C. J. Gross, W. Gelletly, M. A. Bentley, H. G. Price, J. Simpson, K. P. Lieb, D. Rudolph, J. L. Durell, B. J. Varley, and S. Rastikerdar, Phys. Rev. C **44**, R2253 (1991).
[5] M. Weiszflog, K. P. Lieb, F. Christancho, C. J. Gross, A. Jungclaus, D. Rudolph, H. Grawe, J. Heese, K.-H. Maier, R. Schubart, J. Eberth, and S. Skoda, Z. Phys. A **342**, 257 (1992).
[6] E. Galindo, A. Jungclaus, and K. P. Lieb, Eur. Phys. J. A **9**, 439 (2000).
[7] M. K. Kabadiyski, C. J. Gross, A. Harder, K. P. Lieb, D. Rudolph, M. Weiszflog, J. Altmann, A. Dewald, J. Eberth, T. Mylaeus, H. Grawe, J. Heese, and K.-H. Maier, Phys. Rev. C **50**, 110 (1994).
[8] J. N. Scheurer, M. Aiche, M. M. Aleonard, G. Barreau, F. Bourgine, D. Boivin, D. Cabaussel, J. F. Chemin, T. P. Doan, J. P. Goudour, M. Harston, A. Brondi, G. La Rana, R. Moro, E. Vardaci, and D. Curien, Nucl. Instrum. Methods Phys. Res. A **385**, 501 (1997).
[9] J. Gál, G. Hegyesi, J. Molnár, B. M. Nyakó, G. Kalinka, J. N. Scheurer, M. M. Aléonard, J. F. Chemin, J. L. Pedroz, K. Juhász, and V. F. E. Pucknell, Nucl. Instrum. Methods Phys. Res. A **516**, 502 (2004).
[10] Ö. Skeppstedt, H. A. Roth, L. Lindström, R. Wadsworth, I. Hibbert, N. Kelsall, D. Jenkins, H. Grawe, M. Górska, M. Moszyński, Z. Sujkowski, D. Wolski, M. Kapusta, M. Hellström, S. Kalogeropoulos, D. Oner, A. Johnson, J. Cederkäll, W. Klamra, J. Nyberg, M. Weiszflog, J. Kay, R. Griffiths, J. Garces Narro, C. Pearson, and J. Eberth, Nucl. Instrum. Methods Phys. Res. A **421**, 531 (1999).
[11] F. Azaiez, Nucl. Phys. **A654**, 1003c (1999).
[12] J. Simpson, F. Azaiez, G. de France, J. Fouan, J. Gerl, R. Julin, W. Korten, P. J. Nolan, B. M. Nyakó, G. Sletten, and P. M. Walker (EXOGAM collaboration), Heavy Ion Phys. **11**, 159 (2000).
[13] http://www.ganil.fr/exogam
[14] T. K. Alexander and F. S. Goulding, Nucl. Instrum. Methods **13**, 244 (1961).
[15] http://radware.phy.ornl.gov/
[16] D. C. Radford, Nucl. Instrum. Methods A **361**, 297 (1995).
[17] K. S. Krane, R. M. Steffen, and R. M. Wheeler, Nucl. Data Tables **11**, 351 (1973).
[18] B. Schlitt, U. Maier, H. Friedrichs, S. Albers, I. Bauske, P. von Brentano, R. D. Heil, R.-D. Herzberg, U. Kneissl, J. Margraf, H. H. Pitz, C. Wesselborg, and A. Zilges, Nucl. Instrum. Methods Phys. Res. A **337**, 416 (1994).
[19] D. Rudolph, C. J. Gross, A. Harder, M. K. Kabadiyski, K. P. Lieb, M. Weiszflog, J. Altmann, A. Dewald, J. Eberth, T. Mylaeus, H. Grawe, J. Heese, and K.-H. Maier, Phys. Rev. C **49**, 66 (1994).
[20] F. W. N. de Boer, C. A. Fields, L. E. Samuelson, and J. Sau, Nucl. Phys. **A388**, 303 (1982).
[21] M. K. Kabadiyski, F. Christancho, C. J. Gross, A. Jungclaus, K. P. Lieb, D. Rudolph, H. Grawe, J. Hesse, K.-H. Maier,

J. Eberth, S. Skoda, W.-T. Chou, and E. K. Warburton, Z. Phys. A **343**, 165 (1992).
[22] T. Aoki, K. Furuno, Y. Tagishi, S. Ohya, and J.-Z. Ruan, At. Data Nucl. Data Tables **23**, 349 (1979).
[23] E. der Mateosian and A. W. Sunyar, At. Data Nucl. Data Tables **13**, 391 (1974).
[24] E. K. Warburton, C. J. Lister, J. W. Olness, P. E. Haustein, S. K. Saha, D. E. Alburger, J. A. Becker, R. A. Dewberry, and R. A. Naumann, Phys. Rev. C **31**, 1211 (1985).
[25] J. Döring, R. A. Kaye, A. Aprahamian, M. W. Cooper, J. Daly, C. N. Davids, R. C. de Haan, J. Gorres, S. R. Lesher, J. J. Ressler, D. Seweryniak, E. J. Stech, A. Susalla, S. L. Tabor, J. Uusitalo, W. B. Walters, and M. Wiescher, Phys. Rev. C **67**, 014315 (2003).
[26] J. Döring, V. A. Wood, J. W. Holcomb, G. D. Johns, T. D. Johnson, M. A. Riley, G. N. Sylvan, P. C. Womble, and S. L. Tabor, Phys. Rev. C **52**, 76 (1995).
[27] S. L. Tabor, J. Döring, J. W. Holcomb, G. D. Johns, T. D. Johnson, T. J. Petters, M. A. Riley, and P. C. Womble, Phys. Rev. C **49**, 730 (1994).
[28] P. Kemnitz, P. Ojeda, J. Döring, L. Funke, L. K. Kostov, H. Rotter, E. Will, and G. Winter, Nucl. Phys. **A425**, 493 (1984).
[29] A. Dewald, U. Kaup, W. Gast, A. Gelberg, H. -W. Schuh, K. O. Zell, and P. von Brentano, Phys. Rev. C **25**, 226 (1982).
[30] J. Hattula, S. Juutinen, H. Helppi, A. Pakkanen, M. Piiparinen, S. Elfström, and Th. Lindblad, Phys. Rev. C **28**, R1860 (1983).
[31] T. J. Mertzimekis, N. Benczer-Koller, J. Holden, G. Jakob, G. Kumbartzki, K.-H. Speidel, R. Ernst, A. Macchiavelli, M. McMahan, L. Phair, P. Maier-Komor, A. Pakou, S. Vincent, and W. Korten, Phys. Rev. C **64**, 024314 (2001).
[32] S. Chattopadhyay, H. C. Jain, and J. A. Sheikh, Phys. Rev. C **53**, 1001 (1996).
[33] R. A. Kaye, J. B. Adams, A. Hale, C. Smith, G. Z. Solomon, S. L. Tabor, G. Gárcia-Bermúdez, M. A. Cardona, A. Filevich, and L. Szybisz, Phys. Rev. C **57**, 2189 (1998).
[34] D. J. Rowe, *Nuclear Collective Motion, Models and Theory* (Methuen, London, 1970), Part 14.
[35] P. Magierski and R. Wyss, Acta Phys. Pol. B **30**, 815 (1999).
[36] W. Satula and R. Wyss, Phys. Rev. C **50**, 2888 (1994).
[37] V. M. Strutinsky, Nucl. Phys. **A95**, 420 (1967).
[38] P. Ring and P. Shuck, *The Nuclear Many-Body Problem* (Springer-Verlag, Berlin, 1980).
[39] P. Magierski and R. Wyss, Phys. Lett. **B486**, 54 (2000).